Research Article

Synthesis of Titania Doped Copper Ferrite Photocatalyst and Its Photoactivity towards Methylene Blue Degradation under Visible Light Irradiation

Md Noor Arifin[1], Kaykobad Md. Rezaul Karim[1], Hamidah Abdullah[1], Maksudur Rahman Khan[1,2*]

[1]Faculty of Chemical & Natural Resources Engineering, Universiti Malaysia Pahang, Lebuhraya Tun Razak, 26300 Gambang, Kuantan, Pahang, Malaysia
[2]Centre of Excellence for Advanced Research in Fluid Flow, Universiti Malaysia Pahang, Lebuhraya Tun Razak, 26300 Gambang Kuantan, Pahang, Malaysia

Abstract

This paper reports the photocatalytic decomposition of methylene blue (MB) over titania doped copper ferrite, $CuFe_2O_4/TiO_2$ with 50 wt% loading, synthesized via sol-gel method. The synthesized photocatalyst was characterized by X-ray diffraction, UV-vis diffuse reflectance, photoluminescence, and Mott-Schottky (MS) analysis and linear sweep voltammetry (LSV). The catalyst loadings were varied from 0.25-1.0 g/L and the optimum catalyst loading found to be 0.5 g/L. The maximum conversion achieved at this optimized $CuFe_2O_4$ concentration was 83.7 %. The other loadings produced slightly lower conversions at 82.7%, 80.6% and 80.0%, corresponding to 0.25, 1.00, and 0.75 g/L after 3 hours of irradiation. The study on the effect of initial concentration indicated that 20 ppm as the optimum concentration, tested with 0.5 g/L catalyst loading. The spent catalyst was used for the recyclability test and demonstrated a high longevity with a degradation efficiency less than 6 % for each time interval. The novelty of this study lies on the new application of photocatalytic material, $CuFe_2O_4/TiO_2$ on thiazine dye that shows remarkable activity and reusability performance under visible light irradiation. Copyright © 2019 BCREC Group. All rights reserved

Keywords: Copper Ferrite; Photocatalysis; Titania; Methylene Blue

1. Introduction

Heterogeneous photocatalysis is a promising approach for organic pollutant treatment over semiconductors. It has been demonstrated in various applications including the degradation of insecticides, pesticides, dyes, surfactants, chlorinated solvents and non-chlorinated solvents [1]. Another application of this reaction is the degradation of chemical contaminants and microorganisms into water, carbon dioxide and mineral acid [2]. In general, the textile wastewater are treated by physico-chemical treatment processes including chemical precipitation, oxidation, adsorption, and each process of-

* Corresponding Author.
  E-mail: mrkhan@ump.edu.my (M.R. Khan),
  Tel: +6016-9596643, Fax: +609-5492889

fers advantageous and disadvantageous. Biological treatments are frequently applied on the textile effluents, but they are less effective for removing colour from the waste [3,4]. As a result, there are still appreciable amounts of colour in the treated waste effluents when discharged. Another method is the application of inorganic coagulants, such as: polyaluminum chloride (PAC), lime, alum, ferric or ferrous sulfate. Coagulation has been an effective method for the removal of colour especially for wastewater bearing insoluble solids, but huge dosages of chemicals are usually required and finally high amounts of sludge volume have to be disposed off. Consequently, the expenditure of sludge disposal results in relatively high operational costs [5]. Alternatively, the decomposition of organic pollutant such as dye could be carried out under the light source by employing suitable heterogeneous photocatalyst. This is a distinctive advantage of photocatalysis where the solar energy can be utilized in the production of less toxic materials like water and CO_2 [2,6,7].

This photocatalytic reaction is preceded by the absorption of photon by the photocatalyts that possess equal or less band gap energy than the light. Upon fulfilling this first thermodynamic requirement, the electrons at the valence band will be excited to the conduction band [8]. The liberation of electron from the valence band, leaving behind positively charged hole to react with the water molecules to generate hydroxyl radicals, $\cdot OH$ that is responsible to attack the organic pollutant [9]. Besides hydroxyl radicals, the reduction of the oxygen also produces radicals called superoxide anion, $\cdot O_2$ that is active towards the degradation of organic molecules.

One of the most widely used semiconductor-based material, TiO_2 is an active heterogeneous photocatalyst under UV light owing to its wide band gap, approximately 3.3 eV and spectrum of 200-400 nm [10]. Nonetheless, UV light can only be utilized out of 5 % of the solar energy by TiO_2. On the other hand, the visible light makes up more than 40 %, represents a more promising and potential source to be harvested [11]. As one of the metal ferrites, $CuFe_2O_4$ is a spinel-type nanoparticles and possess low band gap [12]. In addition, it is also considered as one of the efficient co-catalysts due to the low cost, high photochemical stability and visible light active photocatalyst [13,14]. However, the sole application of $CuFe_2O_4$ has shown low photocatalytic performance under visible light irradiation owing to high recombination rate of electron-hole (e^-/h^+) pairs. The strategy to cre-

ate a *p-n* heterojunction semiconductor between $CuFe_2O_4$ and TiO_2 was believed to overcome the issue of high recombination rate and providing a migration sites for the charge transfer. The $CuFe_2O_4/TiO_2$ nanocomposite has the advantage of the direct band gap that is positioned near the optimal value of the sun spectrum and its conduction band constituted high energy electrons with the strong reducing ability [12]. In addition, it is an economic option and the Cu and Fe, elements that are environmentally benign.

Therefore, in this work, two main objectives addressed were the synthesis of $CuFe_2O_4/TiO_2$ as a visible light active photocatalyst and its photocatalytic activity. Both strategies, $CuFe_2O_4$ doping and titania incorporation, were undertaken to facilitate the absorption of photons and reducing the recombination of electron-hole (e^-/h^+) pair by effective charge separation. The $CuFe_2O_4/TiO_2$ photocatalysts were then tested with MB at the designed concentration under the visible light irradiation.

2. Materials and Method

2.1 Materials

$Cu(NO_3)_2 \cdot 3H_2O$ (99 %) and $Fe(NO_3)_3 \cdot 9H_2O$ (99 %) with 1:2 molar ratio, copper (II) nitrate, iron (III) nitrate, nitric acid, HNO_3 (65 %), KOH, Agar, TiO_2 (R & M Marketing, Essex, UK), potassium hydroxide (KOH), $NaNO_2$, and sodium sulfite (Na_2S) were of analytical grade (R & M Marketing, Essex, UK) and used without further purification. The reagent grade MB with was purchased from Merck and used without further purification.

2.2 Synthesis of $CuFe_2O_4/TiO_2$

The $CuFe_2O_4/TiO_2$ nanoparticles was synthesized using sol-gel method and the procedure was moderately modified [12]. Firstly, the required amount of $Cu(NO_3)_2.3H_2O$ and $Fe(NO_3)_3.9H_2O$ were dissolved in 400 mL of water which contained HNO_3 (2 M) and 4 g agar, and the solution was allowed to mix for 3 hours under continuous stirring (room temperature). After that, the temperature was raised to 90 ºC and stirred for approximately 3 hours until a green gel was obtained. The gel was then dried at 130 ºC under vacuum for 24 hours and grinded in a mortar. The resulting powder was calcined at 900 ºC with a heating rate of 10 ºC/min for 14 hours [12,15,16]. To prepare $CuFe_2O_4/TiO_2$ photocatalyst, $CuFe_2O_4$ was dispersed in 50 mL distilled water using ultrasound bath (Brand: Elmasonic S; Model:

S10/S10H) and thereafter required amount of commercial TiO_2 was added. The ultrasonication was continued for another 1 hour. Next, the suspension was dried overnight at 100 ºC in an oven. Afterward, the mixture was grinded and calcined at 700 ºC for 3 hours in tubular furnace under N_2 gas atmosphere.

2.3 Characterization of Photocatalysts

XRD (Model: Rigaku MiniFlex II) was used to study the phase and crystallite size of the catalyst at room temperature. The Bragg angle applied was 2θ of 3-80º with a scan step of 0.02. The measurements were carried out at 30 kV and 15 mA using Cu-K_α emission and nickel filter. The crystallite size was determined using Scherrer formula in Equation (1) as follow:

$$D = \frac{K\lambda}{B\cos\theta} \quad (1)$$

where D is the average diameter of the crystals (crystallite size), λ is the wavelength of the X-ray, K is constant (related to crystallite shape), B is the width of the peak (rad.) at half maximum intensity of the diffraction line, and θ is the Bragg angle of the reflection peak [17]. The absorbance spectra of the samples were obtained from the UV-Vis spectrophotometer (Model: Shimadzu UV 2600 UV-Vis-NIR). Finally the electron-hole (h^+/e^-) pairs recombination rates were determined using Luminescence spectrophotometer from Perkin Elmer (Model: LS 55).

The experimental setup for this photocatalytic activity test is self-constructed. The reaction took place in the 500 mL glass reactor, equipped with the outer glass layer for the circulation of the coolant at 20 ºC. The visible light source with 500 W Xe lamp, was positioned at 10 cm above the solution surface. The whole setup was placed in the black metal box in order to avoid any stray current interference with the system.

In the experiment, the amounts of catalyst mixed with the 50 ml of MB solution were varied from 0.0125 to 0.05 g, resulting catalyst loadings of 0.25 to 1 g/L. For this photocatalytic activity test, 20 ppm (20 mg/L) of MB in distilled water was selected as the model dye concentration and the calibration curve was constructed to correlate the absorbance reading from UV-vis and concentration.

Prior to the photocatalytic experiment, the mixture of catalyst and dye solution were stirred in the absence of light for 2 hours. This step was conducted to establish the adsorption-desorption equilibrium between the catalyst and the dye particles. Next, the solution was irradiated with the visible light. For every an hour interval, a 5 ml sample was collected and centrifuged (Model: Eppendorf centrifuge 5810 R). The supernatant was collected in the cuvette and analysed using UV-vis spectroscopy. The unique characteristic wavelength was observed at 665 nm for every standard and sample. The work was proceeded with the investigation on the effect of initial concentrations at 10, 20 and 30 ppm of MB, loaded with 0.5 g/L $CuFe_2O_4/TiO_2$ in each solution. For the recyclability test, the degradation efficiency was calculated using Equation (2) as the following formula:

Degradation efficiency is expressed in Eq.(2)

$$D(\%) = \left(1 - \frac{C}{C_o}\right) \times 100 \quad (2)$$

where C_o is the initial concentration, and C is the concentration at each interval of the measurement.

3. Results and Discussion

3.1 Characterization of $CuFe_2O_4/TiO_2$

Figure 1 depicts the XRD diffractograms of the commercial TiO_2, $CuFe_2O_4$, and $CuFe_2O_4/TiO_2$. The $CuFe_2O_4/TiO_2$ was synthesized following the one to one weight ratio between TiO_2 and $CuFe_2O_4$ and was calcined at 700 ºC. From Figure 1 (a), the TiO_2 peak positions (111), (102), (021), (022), (230), (620), (502), and (532) are in agreement with the JCPDS database (JCPDS Card No. 21-1272). The tetragonal $CuFe_2O_4$ was also calcined at 700 ºC and exhibit characteristic diffraction peaks matching with (101), (112), (200), (202),
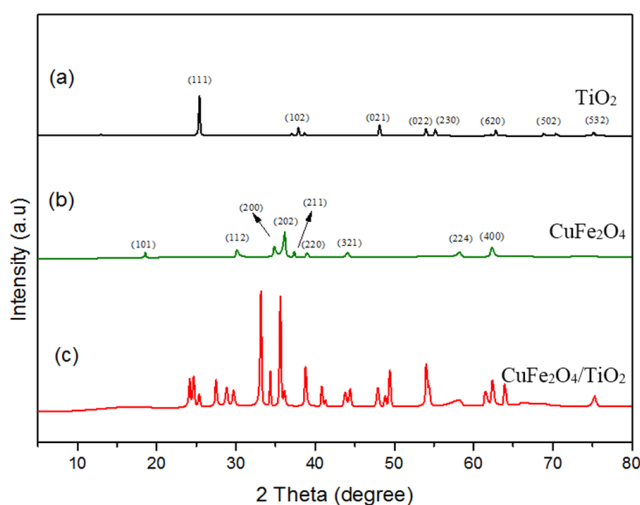
Figure 1. XRD patterns of the photocatalyts; (a) TiO_2, (b) $CuFe_2O_4$, and (c) $CuFe_2O_4/TiO_2$

(211), (220), (321), (224), (400), and (422) (JCPDS Card No. 110 - 200). The similar diffraction peaks for $CuFe_2O_4$ were also indicated in other work [18]. The diffraction peaks of $CuFe_2O_4/TiO_2$ represent tetragonal anatase TiO_2 (JCPDS 111, 102, 021, 022, 230, 620, 502, 532) and tetragonal $CuFe_2O_4$ (JCPDS 112, 202, 402, 221, 200, 312, 321, 224, 116, and 422). Applying the Debye-Scherrer formula, the crystallite size of $CuFe_2O_4$ and $CuFe_2O_4/TiO_2$ photocatalysts are calculated as approximately 59 nm and 64 nm respectively. The slight increase in the crystallite size may be due to the strain effect when the TiO_2 was doped onto $CuFe_2O_4$. The similar observation was also found in the other literatures [18,19]. This calculation was done by considering the 2θ of 36.16^o (maximum intense peak).

Figure 2 shows the UV-vis absorption spectrum for the commercial TiO_2, $CuFe_2O_4$ and $CuFe_2O_4/TiO_2$. As compared to TiO_2 that exhibits a strong activity on the UV-light region, the synthesized catalysts demonstrated a strong absorption for wavelength above 700 nm, indicating the visible light activity. Starting from approximately 400 nm, TiO_2 showed a weak absorption towards the visible light region. Based on the spectral response in Figure 2 (a), a plot of $(\alpha h v)^2$ vs $h v$ was developed as shown in Figure 2 (b). The catalyst is assumed to be the indirect transition type ($n=1/2$) for the determination of the band gap energy of the photocatalysts. The calculated band gaps are 3.25, 1.24, and 1.75 for TiO_2, $CuFe_2O_4$, and $CuFe_2O_4/TiO_2$, respectively. The band gap energy of $CuFe_2O_4/TiO_2$ displays lower value than TiO_2. It has been reported $CuFe_2O_4$ that was also

synthesized via sol-gel method obtain 1.42 eV band gap energy [12], which is close to the obtained value in this work. It is reported that the ideal value of band gap energy should be close to 1.4 eV for the terrestrial application [12]. It is observed that the absorption edge of TiO_2 shifted from 400 nm to 780 nm when it was doped with $CuFe_2O_4$ due to the loading effect.

Photoluminescence spectroscopy and photocurrent measurement were employed to investigate the photoinduced electron-hole (e^-/h^+) pair separation-recombination process. Figure 3 a) presents the spectra of photocatalysts at a wide and strong PL signals, corresponding to the wavelength range of 400-500 nm. The distinguished spectral peaks at 419 and 468 nm correspond to anatase TiO_2 and loading effect of TiO_2 on $CuFe_2O_4$, respectively. Between the two peaks of $CuFe_2O_4/TiO_2$ signal, there is a transition from the oxygen vacancies of TiO_2 with two and one trapped electron to the $CuFe_2O_4$ conduction band (CB) which can be observed at 450 and 466 nm [20]. The $CuFe_2O_4$ band, however, indicated an intense emission due to the recombination of the photoinduced electron-hole pairs, as compared to $CuFe_2O_4/TiO_2$ band which showed a weakening intensities suggesting the loading of TiO_2 on $CuFe_2O_4$ has successfully reduced the recombination rate of electron-hole (e^-/h^+) pairs [21]. The decrease in PL signal may be attributed by the distance of metal ions inter band which becomes narrower, resulting in an energy transfer between the proximal ions. Therefore, a phenomenon that might occur was a concentration quenching process, owing to a non-
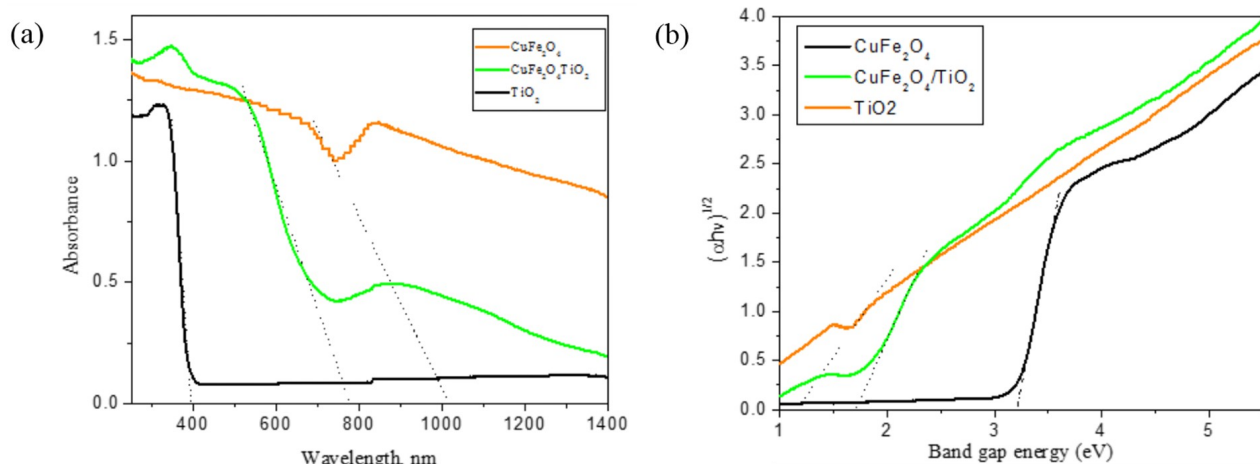
Figure 2. (a) Diffusive reflectance UV-Vis spectra of the TiO_2, $CuFe_2O_4$, and $CuFe_2O_4/TiO_2$ (b) K-M plot for photocatalyts

radiative decay process. For band to band PL signals, the low PL intensity caused a high separation rate of photo-induced charges and, possibly, the higher photocatalytic activity [22].

Upon the light irradiation to the electrodes, the photocurrent rapidly increased and then steadily decreased with time and approached to a constant value, as shown in Figure 3 b). The photocurrent of the $CuFe_2O_4/TiO_2$ electrode was recorded as approximately 12.84 µA indicating the photocatalytic activity of the as prepared $CuFe_2O_4/TiO_2$. The response of the photocatalyst to the applied cathodic current indicated the efficient e^-/h^+ separation and recombination process [23].

Mott-Schottky analyses of (a) $CuFe_2O_4$ and (b) TiO_2 (at 2000 Hz) were conducted in 0.1 M of KCl solution (pH 2.2) and the profile is shown in Figure 4. The negative slope in Mott-

Schottky plot for $CuFe_2O_4$ demonstrated that $CuFe_2O_4$ is a *p*-type semiconductor whereas the positive slope indicated that TiO_2 acted as *n*-type semiconductor. These findings are in agreement with the previous literatures [24,25]. The valence band (VB) position for $CuFe_2O_4$ and conduction band (CB) position of TiO_2 were found as 0.76 V vs NHE and -0.35 V vs NHE respectively. From the results obtained in the band gap measurement, the valence band and conduction band were determined as 3.60 and 0.48 eV for TiO_2 and $CuFe_2O_4$, respectively.

3.2 Photoelectrochemical Activity

Figure 5 exhibits ln C_o/C against time, where C was the concentration of MB at the irradiation time, t and C_o was the concentration
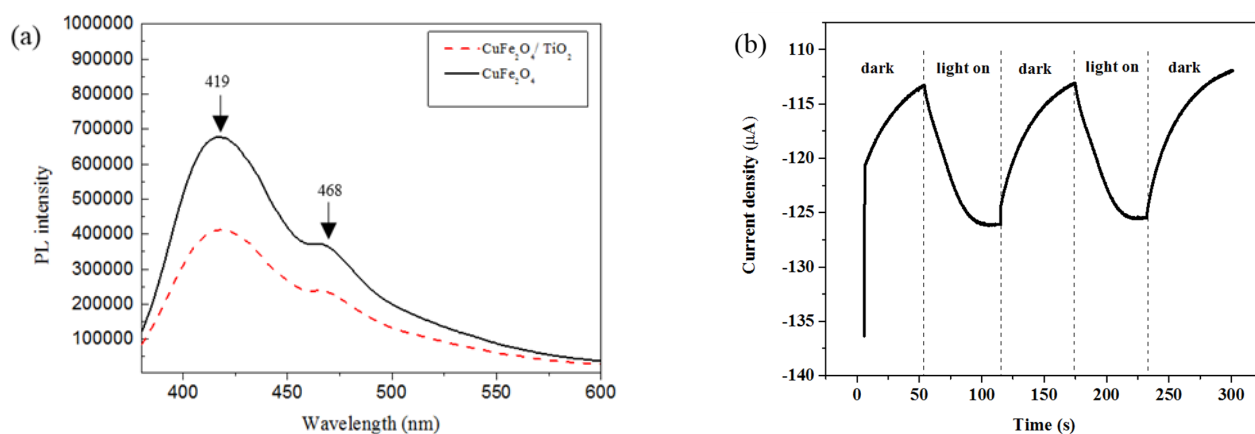
Figure 3. a) Photoluminescence emission spectra of $CuFe_2O_4$ and $CuFe_2O_4/TiO_2$ and b) chronoamperogram of time-dependent photocurrent via several light on-off cycles of $CuFe_2O_4/TiO_2$ electrodes in 0.1 M KCl solution (pH 2.2) at an applied potential of -0.2 V vs NHE.
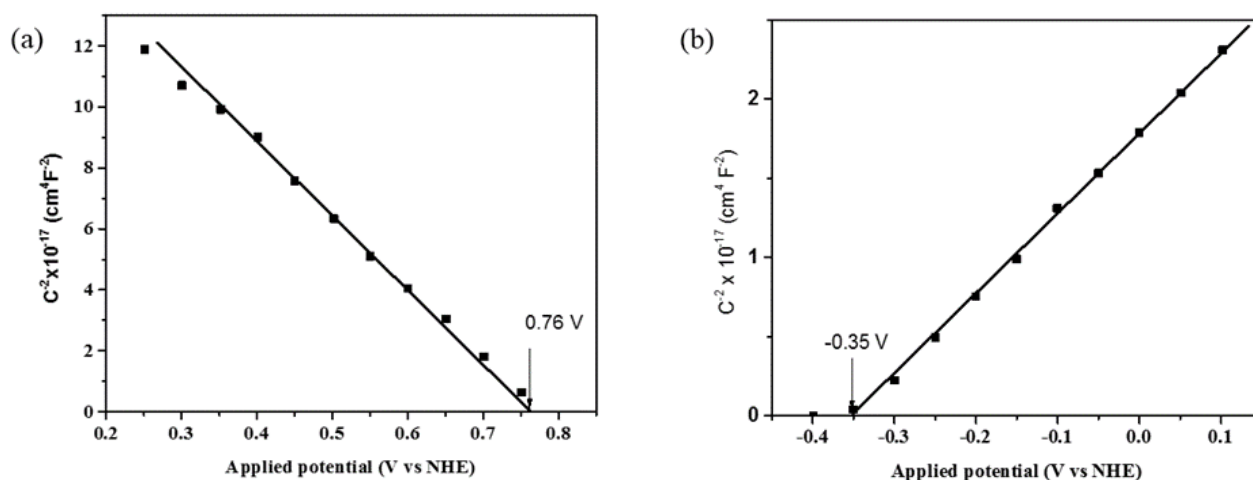
Figure 4. Mott-Schottky results for (a) $CuFe_2O_4$ and (b) TiO_2, analysed at 2000 Hz in 0.1 M KCl solution with pH of 2.2 .

after the 2 hours absorption step at $t = 0$. The investigation on the effects of different photocatalyst loadings on MB degradation was carried out by varying the ratio of catalyst to solution *viz.* 0.25, 0.5, 0.75 and 1.0 g/L. The following mechanism is proposed based on the concept of photocatalytic degradation [26]:

$$CuFe_2O_4/TiO_2 + hv \rightarrow CuFe_2O_4/TiO_2\left(e_{cb}^- + h_{vb}^+\right) \quad (3)$$

$$CuFe_2O_4/TiO_2 + H_2O_{ads} \rightarrow CuFe_2O_4/TiO_2 + OH^- + H^+ \quad (4)$$

$$e_{cb}^- + O_{2,ads} \rightarrow O_2^- \quad (5)$$

$$h_{vb}^+ + OH^- \rightarrow \bullet OH \quad (6)$$

$$\bullet OH + Organic\ complexes(MB) \rightarrow H_2O, CO_2, etc. \quad (7)$$
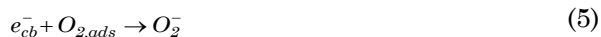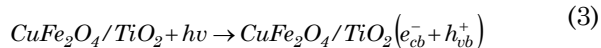
Assuming that the system is irreversible and surface reaction limited (single site), the rate law model, according to the Langmuir-Hinshelwood, can be used to describe the reaction behaviour:

$$-\frac{dC_A}{dt} = -r_A = \frac{kC_A}{1 + K_A C_A} \quad (8)$$

In this study, the selected reactant is an organic dye, MB. The denominator can be simplified into $(1 >> K_A C_A) \sim 1$. As a result, the MB degradation can be described by the Power Law model. For the pseudo first-order reaction kinetics, it follows that:

$$-\frac{dC_A}{dt} = kC_A \quad (9)$$

The following expression is produced upon integration,

$$\ln\left(\frac{C_{Ao}}{C_A}\right) = kt \quad (10)$$

where C_{Ao} = initial concentration (mgL^{-1}), C_A = concentration at time t (mgL^{-1}), t = time (min), k = apparent specific reaction rate (min^{-1}).

The photocatalytic degradation of MB was captured when concentration profiles were fitted to the pseudo first-order kinetics model. Subsequently, the specific reaction rate constant, k was determined from the slope of the linearized plot, constructed from the transient concentration data.

As indicated in Figure 5 (a), the original concentration of the suspension was 20 ppm. The catalytic performance of CuFe$_2$O$_4$/TiO$_2$ on MB at the first hour of reaction showed a high activity of 0.50 g/L, followed by 0.25, 1.00 and 0.75 g/L catalyst loadings. The apparent specific reaction rate, k of 0.5 g/L loading yielded the highest value at 11.3×10^{-3} min^{-1}. This led to the lowest final concentration for the MB suspension with 0.5 g/L loading after 3 hours of reaction. However, the degradation of the MB for all photocatalyt loadings converged to the close conversion percentage, with less than 4 % difference. The high conversion of MB can be attributed to the low band gap energy which improved the photon absorption under the visible light irradiation. This observation is also in line with work by Sumathi *et al.* [27], where the congo red was successfully decomposed by using copper substituted cobalt ferrite with the similar obtained band gap.

The conversion of MB is the highest at 83.7% with the photocatalyst loading of 0.50 g/L, and followed by 0.25, 1.00 and 0.75 g/L. The low dyes conversion at low loading may be due to the limited amount of $\bullet$OH radicals generated [28]. Consequently, there were less MB particles degraded. Nonetheless, the degradation performance was adversely affected when
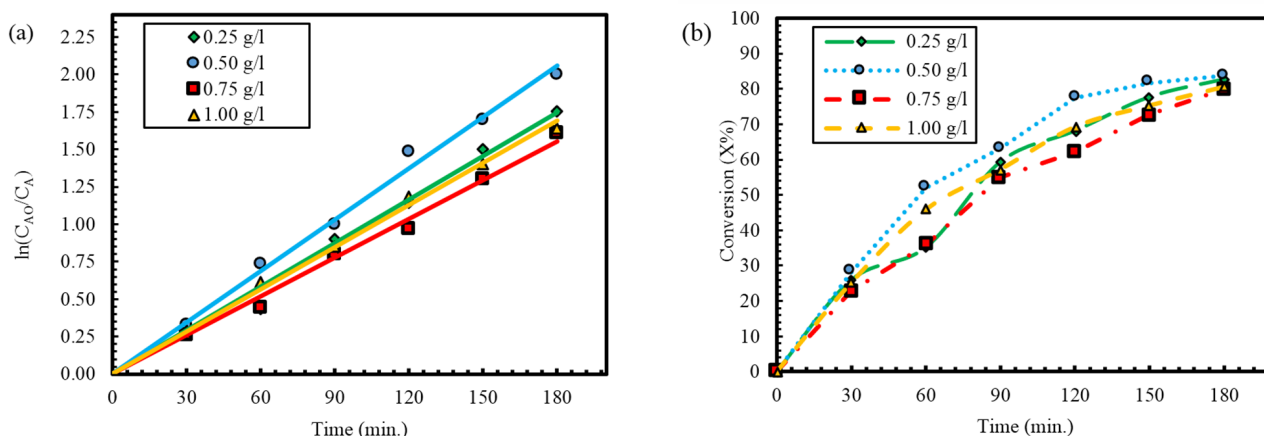
Figure 5. Transient profiles of a) concentration and b) conversion for MB degradation over 0.25, 0.5, 0.75 and 1.0 g/L of CuFe$_2$O$_4$/TiO$_2$ loadings under the 500 W irradiation of visible light source.

the photocatalyst loadings were beyond optimum limit, *i.e.* for 0.75 and 1.0 g/L. This phenomenon can be ascribed to the formation of intermediate species that might have absorbed onto the photocatalysts and cause the blockage. This phenomenon may reduce the available active sites for the dye-photocatalyst absorption [26] and hence reducing the degradation. Another possible explanation to this low performance at high photocatalyst loading is probably due to the light penetration that might have been hindered at the high solid suspension. With the visible light bulb position on the top of the reactor, the top layer of the solution may act as a barrier, disallow the light to reach the lower suspension layer. As a result, photonic activation of photocatalyst was hampered and subsequently reducing the photoexcitation process.

The colour changes from dark to light blue after 3 hours of irradiation were observed. The characteristic absorption was recorded at 665 nm, consistently throughout the entire course of the experiment. The MB absorbance reduced with the visible light exposure time, indicating an increase on the amount of dyes being degraded. Prior to irradiating the solution with the visible light, the system was allowed to reach equilibrium under the 2 hours of stirring. It was found that this pre-reaction step caused the reduction in absorbance at the maximum 15 %, depending on the initial dye concentration.

3.3 Effect of Initial Concentration

As determined previously, the 0.5 g/L photocatalyst loading was found to give the optimal performance in the MB photocatalytic degradation under the visible lights irradiation. Hence, the effect of initial concentrations to the degradation of MB were further sought. In this experiment, three initial concentrations were tested including 20 ppm from the previous test. The resulting concentration and conversion profiles are shown in Figure 6.

It can be seen that the lowest initial concentration, 10 ppm ended with the lowest final concentration after five hour absorption-reaction process taking place. As shown in Figure 6 (b), the optimum initial concentration that produced the highest conversion was 20 ppm. This may be due to the presence of excessive amount of MB molecules at the concentration of 30 ppm has saturated the active sites of $CuFe_2O_4/TiO_2$, hence reducing the photocatalytic activity.

3.4 Photodegradability

The examination of the catalyst longevity was determined by recycling the spent $CuFe_2O_4/TiO_2$ photocatalyst for three consecutive runs, as shown Figure 7. The catalyst was recovered by centrifuging the used catalyst af-
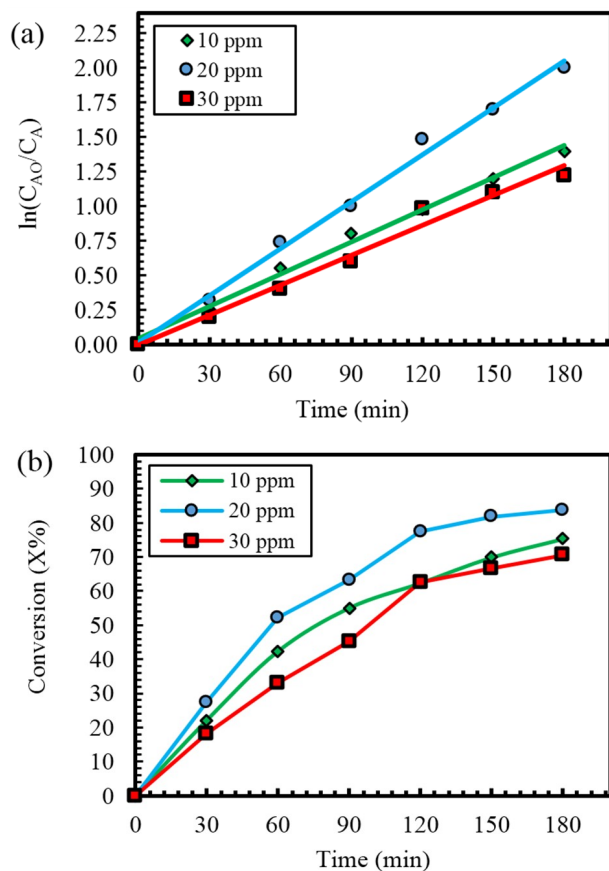
Figure 6. Transient profiles of MB degradation after 3 hours irradiation at three different initial concentrations, 10, 20, and 30 ppm for (a) concentration and (b) conversion.
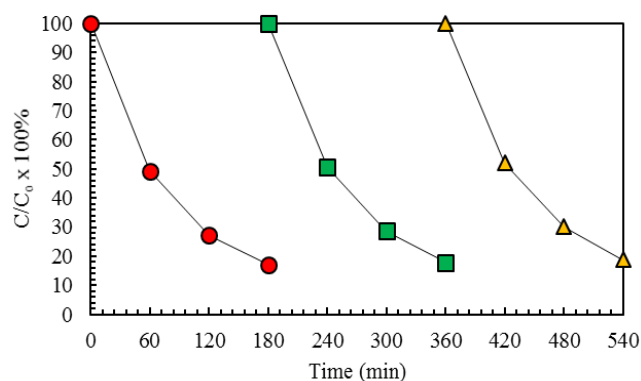
Figure 7. The transient profiles of the recycled spent $CuFe_2O_4/TiO_2$, 0.5 g/L $CuFe_2O_4/TiO_2$ in 10 ppm MB in water for every 3 hours.

ter the photocatalytic reaction. Upon the removal of the supernatant, the catalyst was dried at 80 ºC in the oven for 2 hours before subjected to the next cycle. The degradation efficiency, D (%) of the photocatalyst has reduced marginally throughout the 3 cycles, from 82.9 % to 81.2 %. The synthesized $CuFe_2O_4/TiO_2$ demonstrated a high longevity with a slight decrease in efficiency. This result is supported by the finding from UV-vis diffusive reflectance which suggests an excellent $CuFe_2O_4/TiO_2$ band gap energy (1.75 eV) for the photocatalytic reaction under the visible light. The reaction was further improved by an effective separation of charges, as suggested by the result from photoluminescence spectra. We infer that this photocatalyst can be used for more dyes degradation cycles with an efficient economic option of dyes waste treatment.

4. Conclusion

Titania loaded with $CuFe_2O_4$ was synthesized and employed as a photocatalyst for the photocatalytic degradation of MB, a typical organic pollutant discharged from the textile industry. XRD characterization showed that the final form of the $CuFe_2O_4/TiO_2$ still has retained is anatase phase with crystal diameter ranged from 59 to 64 nm. The obtained UV-vis spectrum indicated that the $CuFe_2O_4$ inclusion has successfully reduced the band gap energy to 1.75 eV which made the catalyst active under the visible light irradiation. Moreover, the results from photoluminescence light study suggested the decreased in recombination rate of electron-hole (e^-/h^+) pair from the intensity profile of $CuFe_2O_4/TiO_2$. Photocatalytic degradation over $CuFe_2O_4/TiO_2$ has effectively decomposed MB within the applied photocatalyst loadings; 0.25-1 g/L, with 0.5 g/L showed the highest conversion at 83.7 %. This study has also found that the optimum concentration of MB to be degraded with 0.5 g/L $CuFe_2O_4/TiO_2$ is 20 ppm. Whereas, the longevity of the photocatalysts were tested for three cycles and the results revealed the degradation efficiency greater than 80%. This novel work presents the new application of $CuFe_2O_4/TiO_2$ on thiazine dye degradation and reusability under visible light irradiation.

Acknowledgments

References

[1] Xu, C., G.P. Rangaiah, X.S. Zhao. (2014). Photocatalytic Degradation of Methylene Blue by Titanium Dioxide: Experimental and Modeling Study. *Industrial & Engineering Chemistry Research.* 53(38): 14641-14649.

[2] Hoffmann, M.R.M., S. T.; Choi, W. (1995). Environmental applications of semiconductor photocatalysis. *Chem. Rev.,* 95(1): 69-96.

[3] Aziz, H.A. Alias, S., Adlan, M.N., Faridah; Asaari, A.H., Zahari, M.S. (2007). Colour removal from landfill leachate by coagulation and flocculation processes. *Bioresour. Technol.* 98(1): 218-220.

[4] Basavarao, V., S. Rammohanrao (2006). Adsorption studies on treatment of textile dyeing industrial effluent by flyash. *Chemical Engineering Journal.* 116(1): 77-84.

[5] Ashtekar, V.S., Bhandari, V.M., Shirsath, S.R., Sai Chandra, P.L.V.N., Jolhe, P.D., Ghodke, S.A. (2014). Dye Wastewater Treatment: Removal of Reactive Dyes Using Inorganic and Organic Coagulants. *Journal of Industrial Pollution Control.* 30(1): 33-42.

[6] Sivakumar, S., Selvaraj, A., Ramasamy, A. K., Balasubramanian, V. (2013). Enhanced Photocatalytic Degradation of Reactive Dyes over $FeTiO_3/TiO_2$ Heterojunction in the Presence of H_2O_2. *Water, Air, & Soil Pollution.* 224(5): 1529

[7] Sobana, N., M. Muruganadham, M. Swaminathan. (2006) Nano-Ag particles doped TiO2 for efficient photodegradation of Direct azo dyes. *Journal of Molecular Catalysis A: Chemical.* 258(1-2): 124-132.

[8] Li, X., Yu, J., Wageh, S., Al-Ghamdi, A.A., Xie, J. (2016). Graphene in Photocatalysis: A Review. *Small.* 12(48): 6640-6696.

[9] Li, L., Wang, X., Lan, Y., Gu, W., Zhang, S. (2013). Synthesis, Photocatalytic and Electrocatalytic Activities of Wormlike $GdFeO_3$ Nanoparticles by a Glycol-Assisted Sol–Gel Process. *Industrial & Engineering Chemistry Research.* 52(26): 9130-9136.

[10] Yan, H., Wang, X., Yao, M., Yao, X. (2013). Band structure design of semiconductors for enhanced photocatalytic activity: The case of TiO_2. *Progress in Natural Science: Materials International.* 23(4): 402-407.

[11] Ng, K.H., Lee, C.H., Khan, M.R., Cheng, C.K. (2016). Photocatalytic degradation of recalcitrant POME waste by using silver doped titania: Photokinetics and scavenging studies. *Chemical Engineering Journal.* 286: 282-290.

[12] Kezzim, A., Nasrallah, N., Abdi, A., Trari, M. (2011). Visible light induced hydrogen on the novel hetero-system CuFe$_2$O$_4$/TiO$_2$. *Energy Conversion and Management*. 52(8-9): 2800-2806.

[13] Yao, Y., Lu, F., Zhu, Y., Wei, F., Liu, X., Lian, C., Wang, S. (2015). Magnetic core-shell CuFe$_2$O$_4$@C$_3$N$_4$ hybrids for visible light photocatalysis of Orange II. *J Hazard Mater*, 297: 224-233.

[14] Li, M., Xiong, Y., Liu, X., Bo, X., Zhang, Y., Han, C., Guo, L. (2015). Facile synthesis of electrospun MFe$_2$O$_4$ (M = Co, Ni, Cu, Mn) spinel nanofibers with excellent electrocatalytic properties for oxygen evolution and hydrogen peroxide reduction. *Nanoscale,* 7(19): 8920-30.

[15] Yan, J., Yang, H., Tang, Y., Lu, Z., Zheng, S., Yao, M., Han, Y. (2009). Synthesis and photocatalytic activity of CuYyFe$_2$-yO$_4$-CuCo$_2$O$_4$ nanocomposites for H$_2$ evolution under visible light irradiation. *Renewable Energy*. 34(11): 2399-2403.

[16] Yang, H., Yan, J., Lu, Z., Cheng, X., Tang, Y. 2009). Photocatalytic activity evaluation of tetragonal CuFe$_2$O$_4$ nanoparticles for the H2 evolution under visible light irradiation. *Journal of Alloys and Compounds*. 476(1-2): 715-719.

[17] Lemine, O.M., (2009). Microstructural characterisation of nanoparticles using, XRD line profiles analysis, FE-SEM and FT-IR. *Superlattices and Microstructures*. 45(6): 576-582.

[18] Karim, K.M.R., Ong, H.R., Abdullah, H., Yousuf, A., Cheng, C.K., Khan, M.M.R. (2018). Electrochemical Study of Copper Ferrite as a Catalyst for CO$_2$ Photoelectrochemical Reduction. *Bulletin of Chemical Reaction Engineering & Catalysis*. 13(2): 236-244.

[19] Uddin, M.R., Khan, M.M.R., Rahman, M.W., Cheng, C.K. (2015). Photocatalytic reduction of CO$_2$ into methanol over CuFe$_2$O$_4$/TiO$_2$ under visible light irradiation. *Reaction Kinetics, Mechanisms and Catalysis*. 116(2): 589-604.

[20] Tahir, M., N.S. Amin, (2015). Indium-doped TiO$_2$ nanoparticles for photocatalytic CO$_2$ reduction with H$_2$O vapors to CH$_4$. *Applied Catalysis B: Environmental*. 162: 98-109.

[21] Miyashita, K., Kuroda, S., Tajima, S., Takehira, K., Tobita, S., Kubota, H. (2003). Photoluminescence study of electron–hole recombination dynamics in the vacuum-deposited SiO$_2$/TiO$_2$ multilayer film with photo-catalytic activity. *Chemical Physics Letters*. 369(1-2): 225-231.

[22] Liqiang, J., Yichun, Q., Baiqi, W., Shudan, L., Baojiang, J., Libin, Y., Wei, F., Honggang, F., Jiazhong, S. (2006). Review of photoluminescence performance of nano-sized semiconductor materials and its relationships with photocatalytic activity. Solar Energy Materials and Solar Cells, 90(12): 1773-1787.

[23] Yan, J., Gu, J., Wang, X., Fan, Y., Zhao, Y., Lian, J., Xu, Y., Song, Y., Xu, H., Li, H. (2017). Design of 3D WO$_3$/h-BN nanocomposites for efficient visible-light-driven photocatalysis. *RSC Advances*. 7(40): 25160-25170.

[24] Taffa, D.H., Dillert, R., Ulpe, A.C., Bauerfeind, K.C.L., Bredow, T., Bahnemann, D.W., Wark, M. (2016). Photoelectrochemical and theoretical investigations of spinel type ferrites (MxFe$_3$-xO$_4$) for water splitting: a mini-review. *Journal of Photonics for Energy*. 7(1): 012009

[25] Wisitsoraat, A., Tuantranont, A., Comini, E., Sberveglieri, G., Wlodarski, W. (2009). Characterization of n-type and p-type semiconductor gas sensors based on NiO$_x$ doped TiO$_2$ thin films. *Thin Solid Films*. 517(8): 2775-2780.

[26] Ng, K.H., C.K. Cheng, (2016). Photo-polishing of POME into CH4-lean biogas over the UV-responsive ZnO photocatalyst. *Chemical Engineering Journal*. 300: 127-138.

[27] Kirankumar, V.S., B. Hardik, S. Sumathi, (2017). Photocatalytic degradation of congo red using copper substituted cobalt ferrite. *IOP Conference Series: Materials Science and Engineering*. 263: 022027

[28] Cheng, C.K., Deraman, M.R., Ng, K.H., Khan, M.R. (2016) Preparation of titania doped argentum photocatalyst and its photoactivity towards palm oil mill effluent degradation. *Journal of Cleaner Production*. 112: 1128-1135.